J Inorg Organomet Polym (2015) 25:1582–1589
DOI 10.1007/s10904-015-0262-x

COMMUNICATION

Methyl orange removal from wastewater using $[Zn_2(oba)_2(4\text{-bpdh})]\cdot 3DMF$ metal–organic frameworks nanostructures

Amir Reza Abbasi[1] · Mohammadreza Yousefshahi[1] · Azadeh Azadbakht[2] · Ali Morsali[3] · Mohammad Yaser Masoomi[3]

Received: 25 May 2015 / Accepted: 24 July 2015 / Published online: 15 August 2015

Abstract A porous coordination polymer, $[Zn_2(oba)_2(4\text{-bpdh})]\cdot 3DMF$ (**TMU-5**) upon silk yarn, has been synthesized under ultrasound irradiation. We here present a textile for the adsorptive removal methyl orange from wastewater using three-dimensional porous Zn(II)-based metal–organic framework (**TMU-5**) and silk fibers. The effect of sequential dipping steps in growth of **TMU-5** upon fiber has been studied. These systems depicted a decrease in the size accompanying a decrease in the sequential dipping steps. The samples were characterized with powder X-ray diffraction (XRD), Fourier transform infrared spectroscopy spectra and scanning electron microscopy. XRD analyses indicated that the prepared **TMU-5** on silk fibers were crystalline.

Keywords Ultrasound irradiation · Metal–organic framework · Wastewater · Methyl orange

✉ Amir Reza Abbasi
ar.abbasi@razi.ac.ir

✉ Ali Morsali
Morsali_a@modares.ac.ir

[1] Faculty of Chemistry, Razi University, Kermanshah 67194, Islamic Republic of Iran

[2] Department of Chemistry, Faculty of Science, Khorramabad Branch, Islamic Azad University, Khorramabad, Iran

[3] Department of Chemistry, Faculty of Sciences, Tarbiat Modares University, P.O. Box 14155-4838, Tehran, Iran

1 Introduction

The field of metal–organic frameworks (MOFs), which are also called porous coordination polymers (PCPs), has been growing tremendously over the last two decades [1, 2]. This fascinating class of crystalline hybrid materials, which are formed by association of metal centers or clusters linked together by organic ligands, offers a unique chemical versatility combined with a designable framework and an unprecedentedly large and permanent inner porosity [3–5]. Metal–organic frameworks have unquestionably enormous potential for many practical structure-related applications. This includes the more traditional areas of storage, separation or controlled release of gases, drug delivery, sensing and catalysis as well as the adsorptive removal of hazardous materials, which are based on the pore size and shape as well as the host–guest interactions involved [6–12]. Presently, environmental pollution is one of the most problematic issues worldwide. There have been many trials both to reduce pollution and to eliminate the polluting materials from the environment. Common hazardous materials that exist in our environment are dyes, personal care products, pharmaceuticals and so on. Therefore, extensive studies have been done on the separation of various gaseous and liquid components with MOFs. However, the majority of these applications are based on the ability of MOFs to behave as hosts for certain molecules. Apart from their use as bulk materials, these frameworks could be processed as supported homogeneous porous thin films on various surfaces. Controlling the assembly of MOFs thin films on different substrates is currently recognized as one of the most important issues in the synthesis of functional materials [13]. Different strategies have been developed in the literature to fabricate thin films of MOFs. These technical approaches can be

grouped in several ways such as surface functionalization [14], layer-by-layer (LBL) [15] and electrospun nanofibrous filters [16].

In this work we report the layer-by-layer deposition of a microporous Zn(II)–MOF material on the surface of natural fiber with –COOH surface functionalization under ultrasound irradiation. The advantage of ultrasonic method is the homogeneous coating of small nanostructures with a narrow size distribution [17, 18]. In anchoring MOFs to surfaces (SURMOFs), the first step is the functionalization of substrate or self-assembled monolayers (SAMs) and the second step is the growth of MOF. Two different methods for the synthesis of MOF thin films have been recently developed: direct growth from solvothermally pretreated solutions, [19–21] and LBL growth from molecular precursors. Deposition of microcrystalline MOF at alumina [22, 23], silica [22] and on surfaces of flexible organic polymers [24] were reported, but in this work we used silk fibers as substrate, thus due to existence of –COOH groups on the surface of these silk fibers no SAM formation was required and in a very simple and effective procedure at ambient pressure and temperature, $[Zn_2(oba)_2(4\text{-bpdh})]\cdot 3DMF$ (**TMU-5**) coating of the silk fibers were done successfully by LBL technique. **TMU-5** shows narrow, three-dimensional interconnected pores (aperture size of 4.4×6.2 Å^2) that are also functionalized with azine groups. For augment of porosity in **TMU-5** upon fiber, we successfully tested its porosity with guest molecules by suspending it in an aqueous solution of methyl orange (**MO**). **MO** is one of the well-known acidic/anionic dyes, and has been widely used in textile, printing, paper, food and research laboratories. The deposition of MOF thin films on flexible surfaces might be a new path for the fabrication of functional materials for different applications, such as removal of hazardous materials, protection layers for working clothes and gas separation in the textile industry.

2 Experimental Section

2.1 Materials and Physical Techniques

All reagents and solvents were used as supplied by Merck Chemical Company and used without further purification. The silk fiber (63 6 6.7 Tex and 240 twists per meter) was obtained from Guilan Silk Company. The natural silk fibers were pre washed using an aqueous solution containing NaOH (pH 9), at 25 °C for 5 min, followed by washed several times with water and dried at ambient temperature. X-ray powder diffraction (XRPD) measurements were done on a Philips X'pert diffractometer with monochromatic Cu Kα radiation. The simulated XRD powder pattern based on single crystal data were prepared using Mercury software [25]. The samples were characterized with a scanning electron microscope (SEM, Philips XL 30 and S-4160) with gold coating. Ultrasonic generators were carried out on a Eurosonic 4D (continuous mode, output power: 350 W). Ultrasonic generators have water circulation system and double jacketed vessel. The effects of sonication in growth of the **TMU-5** upon fiber were studied in 350 W. In situ UV/vis spectrum experiment has been carried out on a PG Instruments, T80 + UV/vis/NIR spectrophotometer within the wavelength range 190–800 nm, using the same solvent in the examined solution as a blank. Infrared spectra were taken with a FT-IR Bruker, vector 22 spectrometer using KBr pellets in the 400–4000 cm^{-1} range.

2.2 Syntheses of TMU-5 Upon Silk Surfaces

The ligand 2,5-bis(4-pyridyl)-3,4-diaza-2,4-hexadiene (4-bpdh) was synthesized according to previously reported methods [26]. The growth of **TMU-5** upon silk fiber was achieved by sequential dipping in alternating bath of aqueous $Zn(NO_3)_2.6H_2O$ (0.189 g, 0.64 mmol) and DMF solution of 4-bpdh (0.238 g, 1 mmol) and 4,4′-oxybisbenzoic acid (H_2oba) (0.254 g, 1 mmol) under ultrasound bath. Before the experiment began, silk fibers were immersed in an alkaline solution. In alkaline pH, the surface of fiber becomes negatively charged due to deprotonation of the carboxylic group present at the fiber's surface [27]. The first layer was fabricated by immersing the silk-COO^- surface into an solution of Zn(II) and then in solution of ligands (1 cycle). When negative fiber was immersed in an aqueous solution of zinc(II) nitrate, Zn(II) ions are attracted to the fiber surface [17]. The dipping step in 4-bpdh/H_2oba solutions allowed the formation of **TMU-5** and initiated the formation of new **TMU-5** particles, as illustrated in Fig. 1.

The results show that sequential dipping in alternating baths of aqueous Zn(II) and 4-bpdh/H_2oba leads to a stepwise deposition of **TMU-5** multilayers. The thickness of the multilayers was increased with the increase of the deposition cycles [17]. The dipping step in each Zn(II) and 4-bpdh/H_2oba solutions was 1.5 min followed by some rinses in pure DMF each for 1 min. In order to investigate the deposition of the first 15 MOF layers on the surface of the silk fiber the substrate was dipped alternatively into SBU- and linker solution with washing with DMF in between [28].

3 Results and Discussion

3.1 Fourier Transform Infrared Spectroscopy (FT-IR) and X-ray Powder Diffraction (XRPD)

Due to the small amount and thickness of the deposited MOF film, the standard technique of FT-IR is suited for the

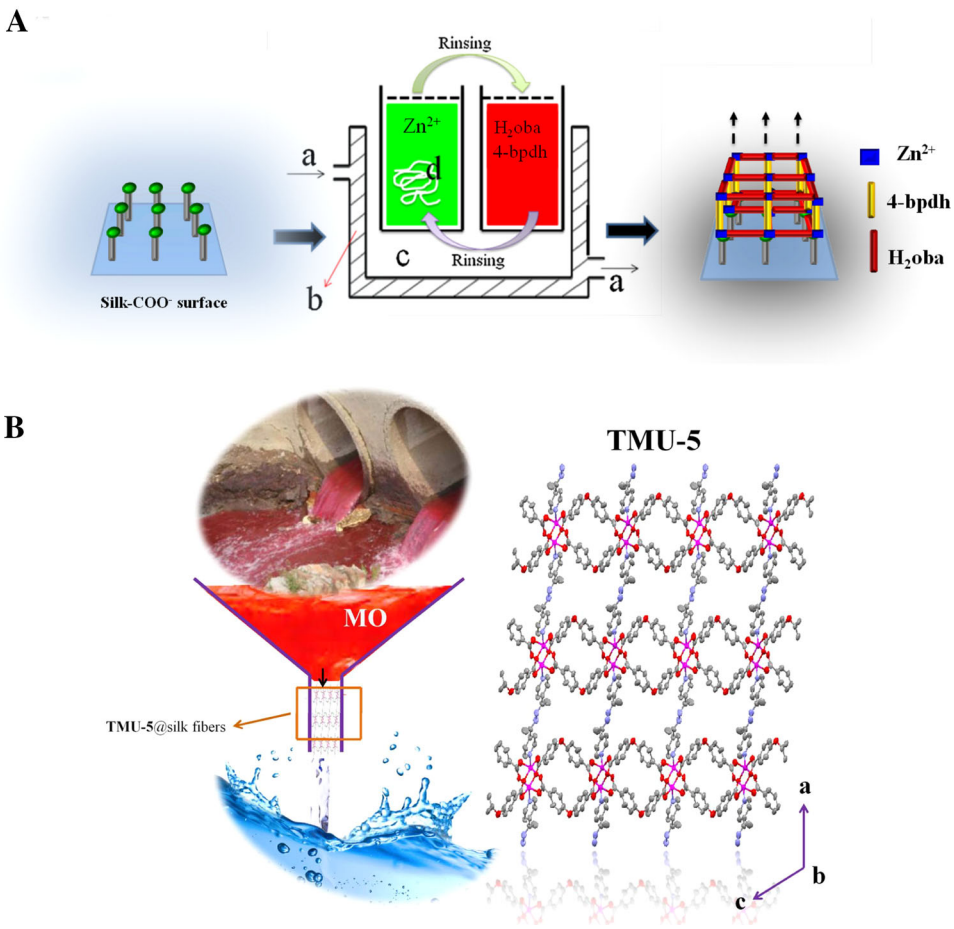

Fig. 1 **a** Schematic representation of the formation mechanism of **TMU-5** upon silk fiber: *a* water circulation, *b* double jacketed vessel, *c* ultrasound bath and *d* silk yarn. **b** Schematic of active membrane device proposed and layers of Zn(II)-oba pillared by 4-bpdh (**TMU-5**)

investigation of film quality. Therefore, after each deposition cycle an absorption spectrum of the dried substrate was recorded. The increase of the intensity of the vibrational bands ($\upsilon = 779$, 879, 2360, 2486 and 2923 cm^{-1}) from **TMU-5** phase is proportional to the number of performed deposition cycles. It can be concluded that the characterization of MOF films with a low number of performed deposition cycles can be better achieved using the FT-IR spectra than XRPD due to its limitation in detection of films with a thickness <40 nm [28]. The change of the intensity was observed after the first deposition cycle on the silk surface. Although the observed change of the intensity is small, the intensity increases continuously with each further deposition cycle (Fig. 2). The linear increase of the absorbance indicates a regular assembly of the cationic and anionic building blocks. FT-IR data (KBr pellet, ν/cm^{-1})-selected bands: 658(m), 777(m), 1091(m), 1159(s), 1238(vs), 1408(vs), 1501(m), 1608(vs), 1677(s) and 3428(w-br).

To determine the crystal phase of **TMU-5** formed upon silk fiber, XRPD measurements were carried out over the diffraction angle (2θ) of 0–50°. Figure 3 shows the XRPD patterns; simulated from single crystal X-ray data of **TMU-5** (A), as-synthesized **TMU-5** (B), pristine silk fibers (C) and **TMU-5** upon silk after applying 15 (D). Figure 3e shows the X-ray powder diffraction patterns of **TMU-5** upon silk soaked in an aqueous solution (10^{-4} mol L^{-1}) of methyl orange (**MO**) at room temperature for 3 days. It is worth noting that when the crystals were soaked in the solution for about 3 days, most of the peaks in the XRPD data distinctly weakened. The unusual phenomenon can be well explained by the high amount of **MO** in **TMU-5**, which has a significant impact on the sensitivity of the X-ray analysis. The eight major peaks found at 6.70°, 7.70°, 9.35°, 10.95°, 12.20°, 14.70°, 14.77° and 15.94° on the two theta scale correspond respectively to the (200), (002), ($20\bar{2}$), (202), (111), ($11\bar{2}$), (310) and ($31\bar{2}$) crystal planes. Acceptable matches with slight difference in 2θ, were observed between the simulated XRPD pattern and the experimental data [26]. It is also noted that for the Fig. 3d, e the relative intensities of ($20\bar{2}$), (202), (111), ($11\bar{2}$), (310) and ($31\bar{2}$) reflections are, respectively, larger or smaller than that in the simulated pattern [29]. The results indicated that **TMU-5** formed on the silk fiber (Fig. 3) and the crystallinity of the coated $[Zn_2(oba)_2(4\text{-bpdh})]\cdot 3DMF$ MOF films were increased by increasing the

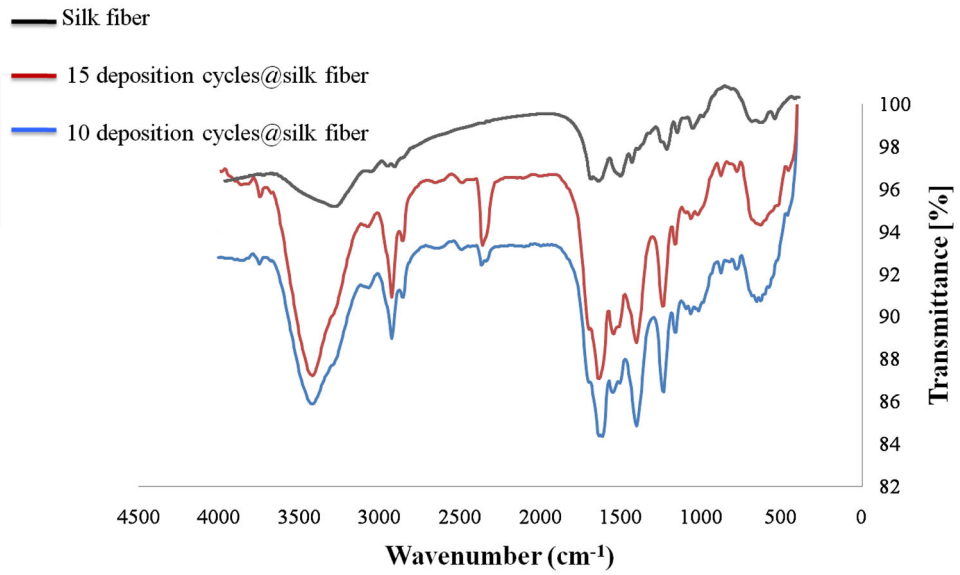

Fig. 2 FT-IR spectra of pure silk fiber and silk fiber containing **TMU-5** after applying 10 and 15 deposition cycles (Color figure online)

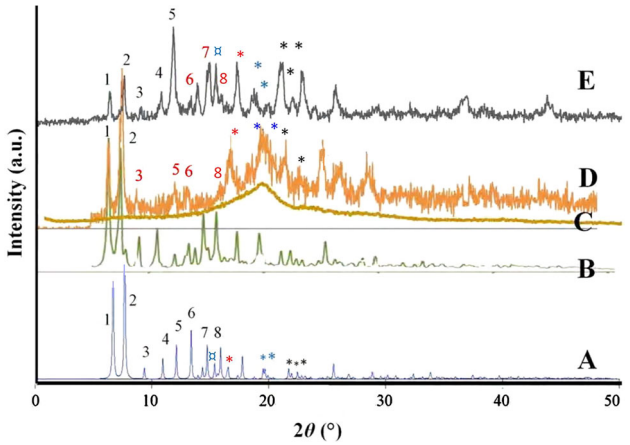

Fig. 3 **a** Simulated pattern based on single crystal data of XRPD pattern of **TMU-5**, **b** as-synthesized **TMU-5**, **c** the pure silk fiber, **d** **TMU-5** upon silk after applying 15 deposition cycles, **e** XRPD patterns of **TMU-5** upon silk soaked in an aqueous solution (10^{-4} mol L^{-1}) of **MO** at room temperature for 3 days

cycles of layer by layer coating of **TMU-5** on the silk fibers (Fig. 2) [17], the wide peak at 17–23° corresponds to the silk substrate [17, 30]. The obtained pattern match with the pattern of monoclinic **TMU-5**, space groups *C2/c* with the lattice parameters $a = 26.8080(14)$ Å, $b = 8.1923(5)$ Å, $c = 23.3025(16)$ Å and $z = 8$ [26].

3.2 Effects of Sequential Dipping Steps

Particle sizes and morphology of nanoparticles are depending on sequential dipping [31]. Effect of different sequential dipping in growth of **TMU-5** upon fiber were studied at pH 9. The results suggest that with increasing the fiber dipping steps into SBU- and linker solution, growth takes place on more nuclei, the Zn(II) and 4-bpdh/H_2oba attraction increases, and subsequently the concentration and size of **TMU-5** particles upon silk fiber increases [27].

For the sake of investigating the morphology of the prepared coating samples, the SEM images of samples were studied. The SEM images of the non-modified natural fiber were compared with images after applying 4 and 15 deposition cycles of **TMU-5** upon silk fiber (Fig. 4a–c). The surface of the individual fibers is covered by a continuous film of separated crystals with an average size of 207 and 310 nm for 4 and 15 deposition cycles, respectively, without defects. However, the SEM images with a low magnification also exhibit areas with big agglomerates of the deposited MOF. This can be understood by considering the possible storage effect of the unreacted material between the fibers. The wavelength-dispersive X-ray (WDX) mapping of the surface shows the uniform distribution of Zn throughout the whole substrate surface.

3.3 Ultrasound Effects

In order to investigate the role of sonicating on the nature of products, blank reaction was performed without ultrasound irradiation (Fig. 4d). In this reaction, **TMU-5** particles on silk fibers were prepared by sequential dipping steps without sonicating. The average particle size for ultrasound method is around 207 nm (Fig. 4B) while, the average particle size for blank sample (Fig. 4d) in similar conditions is over 245 nm. Results show that in present of ultrasound radiation, particle sizes are in a low range. This finding has already been observed in other studies on ultrasound-assisted synthesis of nano-particles [30]. The sonochemical irradiation of a liquid causes two primary

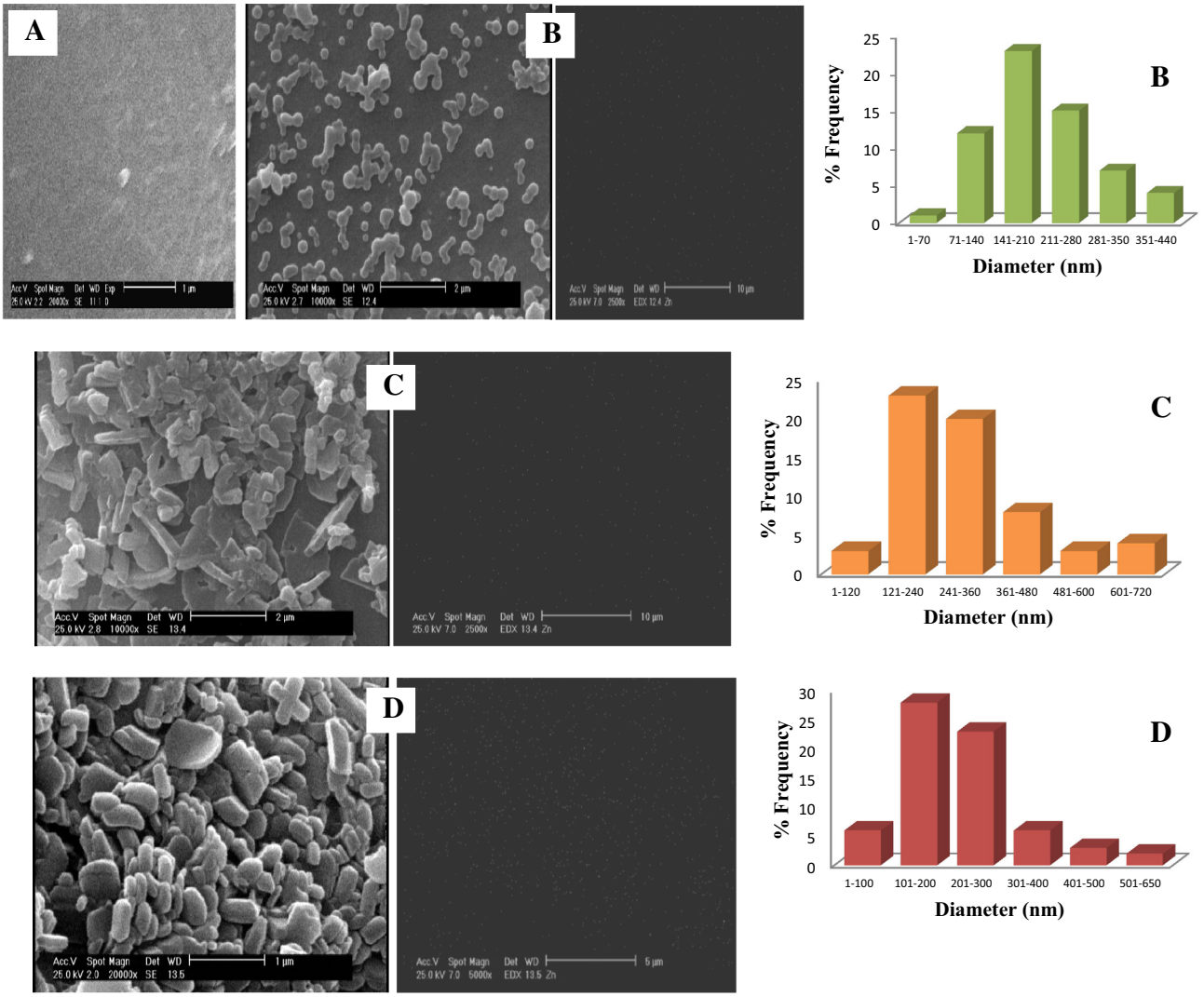

Fig. 4 **a** SEM image of the pristine silk fiber. SEM photographs, the corresponding particle size distribution histograms and corresponding wavelength-dispersive X-ray (WDX) analysis of **TMU-5** upon silk after applying 4 (**b**) and 15 deposition cycles (**c**) under ultrasound irradiation, **d** four deposition cycles without ultrasound irradiation

effects, namely, cavitations (bubble formation, growth, collapse) and heating. When the microscopic cavitations bubbles collapse near the surface of the solid substrate, they generate powerful shock waves and microjets that cause effective stirring/mixing of the adjusted layer of liquid. The after-effects of the cavitations are several hundred times greater in heterogeneous systems than in homogeneous systems [31]. In our case, the ultrasonic waves promote the fast migration of the newly-formed nanoparticles to the fabric's surface. There is reliable evidence that applying ultrasound not only induces nucleation, but also increases reproducibility.

Another effect of ultrasound on nucleation is shortening the induction time between the establishment of supersaturation and the onset of nucleation and crystallization. The cavitation events allow the excitation energy barriers associated with nucleation to be surmounted, in which case it should be possible to correlate the number of cavitation and nucleation events in a quantitative way [32]. It has been suggested that nucleation caused by scratching the walls of a vessel containing a supersaturated solution with a glass rod spatula could be the result of cavitation [31].

3.4 Adsorption Affinity

The porosity of MOF films deposited on substrate surfaces is an important point concerning the possible use of such functional materials for different purposes. **TMU-5** shows three-dimensional (3D), interconnected, narrow pores (Fig. 1b) (size: 5.6 × 3.8 $Å^2$, including van der Waals

radii). We observed that the combination of pore size (narrow and interconnected) and pore functionalization (azine groups) favor the host–guest interactions [26]. For augment of porosity in **TMU-5** upon silk, we successfully tested its porosity with **MO** molecules by suspending it in an aqueous solution of methyl orange. The silk fiber containing 1.0 g of **TMU-5** was immersed in a sufficient amount of a wastewater containing 0.0245 mmol **MO** in a small sealed flask at room temperature and was monitored in real time with a camera (Fig. 5a). The dark red solutions of **MO** fade slowly to colorless, while the **TMU-5** upon silk gets darker (93 h). We tested for the amount of **MO** that can be inserted in the pores. The **MO** content was estimated by XRPD (Fig. 3e) and UV/vis spectroscopy (Fig. 5b) [33]. The change of intensity and width indicates that the resulting solid **TMU-5** upon silk retains the host framework crystallinity as **MO** molecules diffused in. To explore the absorption ability of the **TMU-5** to **MO**, silk fiber containing 1.3 mg of **TMU-5** was immersed in 0.0245 mmol **MO** solutions and were monitored in real time with UV/vis spectroscopy. The entry of **MO** into the **TMU-5** host frameworks leads to a distinct decrease in intensity of the adsorption band at 477 nm, which corresponds to the concentration of MO (Fig. 5b). The adsorption of **MO** by **TMU-5** can be explained by two phenomena. First, **MO** can undergo an acid–base type reaction with the free carboxylic acid and azine groups. Second, **MO** can bind to carboxylic acid and azine groups by hydrogen bonding, increasing the sorption capacity. Adsorption of **MO** was spontaneous and endothermic, and the entropy (the driving force of the adsorption) increases with the adsorption of **MO** [34]. Entropic hydrophobic interactions occur when a guest replaces the water within a cavity. An increase in entropy increases the favorability of the process.

3.5 Release Assays

The encapsulated guest could be easily removed from the frameworks upon immersion of guest upon MOFs in organic solvents. When the crystals of **MO** upon **TMU-5** upon fibers were soaked in dry ethanol, the color of the crystals changed gradually from dark yellow to orange and light yellow in about 14 days, and the color of the ethanol

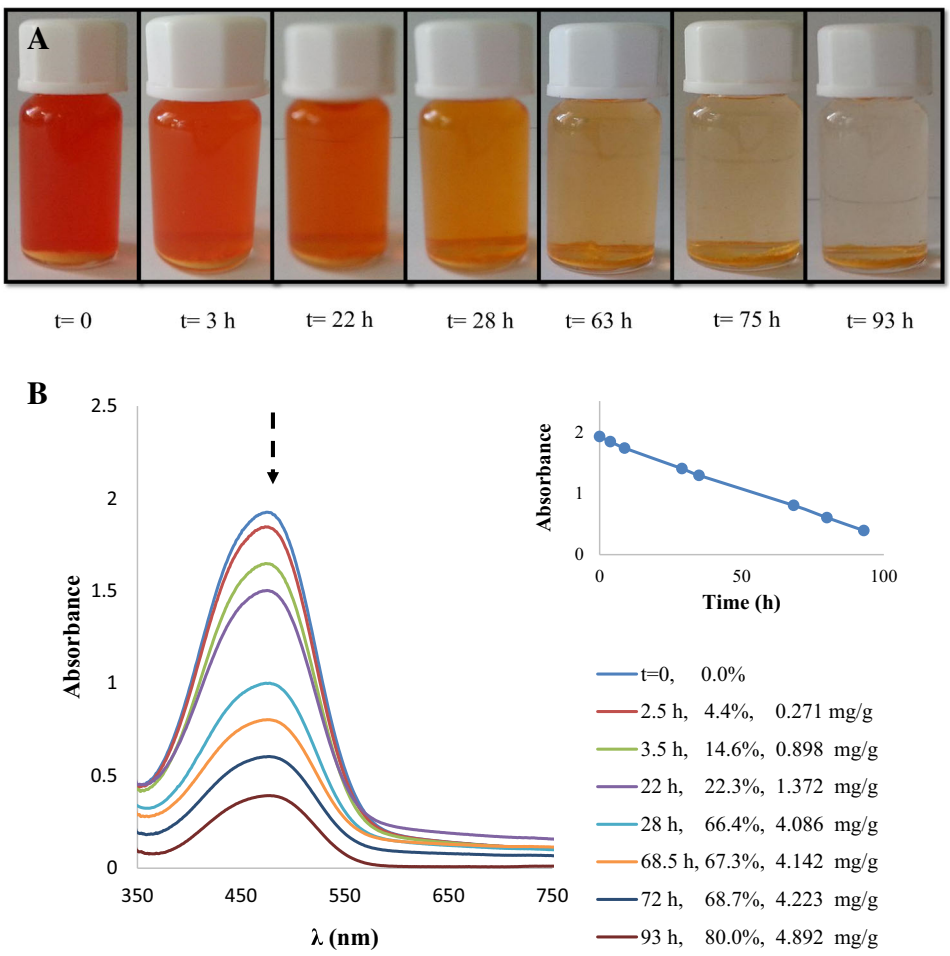

Fig. 5 **a** Photographs showing the visual color change when 10 mg of **TMU-5** upon silk was immersed in 3 mL of an aqueous solution of **MO** (0.007 mol L^{-1}). No further change in color occurred after 93 h, **b** temporal evolution of UV/vis absorption spectra for the loading of **MO** from **TMU-5** upon silk. The percent and concentration of **MO** inside MOF was measured by UV/vis spectroscopy (Color figure online)

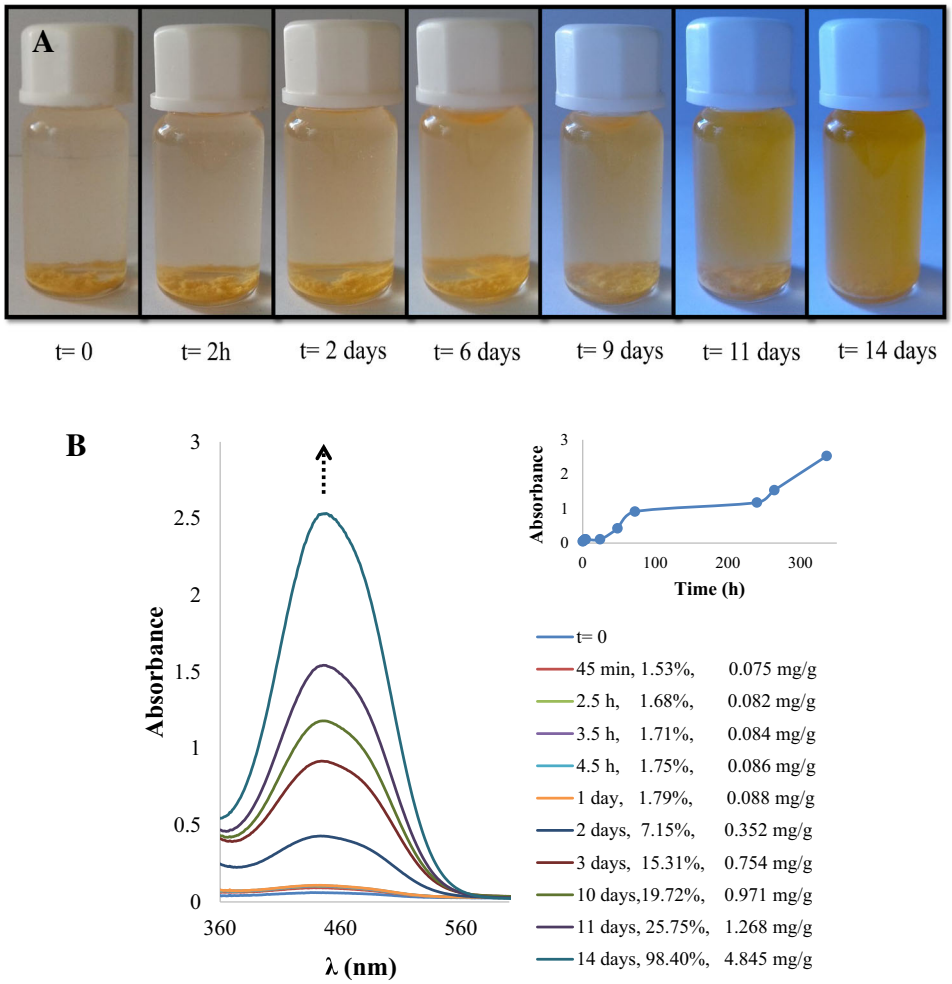

Fig. 6 **a** Photographs showing the **MO** release process when 50 mg of **MO** upon **TMU-5** upon fiber were immersed in EtOH (3 ml), **b** temporal evolution of UV/vis absorption spectra for the delivery of **MO** from **TMU-5** upon silk containing **MO**. The percent and concentration of **MO** in the solution was measured by UV/vis spectroscopy (Color figure online)

solutions deepened gradually from colorless to darker yellow (Fig. 6a). To further investigate the kinetics of the guest delivery of the framework, UV/vis spectra were recorded at room temperature. The temporal evolution UV/vis spectrum for **MO** in ethanol solution, which shows λ_{max} at 442 nm, becomes stronger with increasing **MO** content (Fig. 6b). The delivery of **MO** in ethanol increases with time, indicating that the **MO** release is governed by the host–guest interaction. Methyl orange release from **TMU-5** occurs within 14 days and then moves toward the equilibrium state.

4 Conclusions

In summary, we reported the fabrication of $[Zn_2(oba)_2(4\text{-bpdh})]\cdot 3DMF$ (**TMU-5**) metal–organic framework nanostructures upon silk fiber using layer-by-layer method at ambient pressure and temperature. Due to existence of –COOH groups on the surface of the silk fibers no self-assembled monolayer formation was required. XRPD analyses indicated that the prepared **TMU-5** MOF on silk fibers were crystalline. The deposition of MOF thin films on natural fiber surfaces might be a new path for the fabrication of functional materials for different applications, such as protection layers for working clothes and gas separation materials in the textile industry. **TMU-5** upon silk may indeed is suitable for applications requiring frequent loading and unloading of guests.

Acknowledgments Support of this investigation by Iran National Science Foundation: INSF and Razi University of Kermanshah are gratefully acknowledged.

References

1. F.A. Almeida Paz, J. Klinowski, S.M.F. Vilela, J.P.C. Tome, J.A.S. Cavaleiro, J. Rocha, Ligand design for functional metal-organic frameworks. Chem. Soc. Rev. **41**, 1088–1110 (2012)
2. H.C. Zhou, J.R. Long, O.M. Yaghi, Introduction to metal-organic frameworks. Chem. Rev. **112**, 673–674 (2012)
3. S. Kitagawa, S. Noro, T. Nakamura, Pore surface engineering of microporous coordination polymers. Chem. Commun. **7**, 701–707 (2006)

4. D. Maspoch, D. Ruiz-Molina, J. Veciana, Old materials with new tricks: multifunctional open-framework materials. Chem. Soc. Rev. **36**, 770–818 (2007)
5. J.J.T. Perry, J.A. Perman, M.J. Zaworotko, Design and synthesis of metal-organic frameworks using metal-organic polyhedra as supermolecular building blocks. Chem. Soc. Rev. **38**, 1400–1417 (2009)
6. R.B. Getman, Y.S. Bae, C.E. Wilmer, R.Q. Snurr, Review and analysis of molecular simulations of methane, hydrogen, and acetylene storage in metal-organic frameworks. Chem. Rev. **112**, 703–723 (2012)
7. H.B. Tanh Jeazet, C. Staudt, C. Janiak, Metal-organic frameworks in mixed-matrix membranes for gas separation. Dalton Trans. **41**, 14003–14027 (2012)
8. J. Sculley, D. Yuan, H.-C. Zhou, The current status of hydrogen storage in metal–organic frameworks—updated. Energy Environ. Sci. **4**, 2721–2735 (2011)
9. M. Yoon, R. Srirambalaji, K. Kim, Homochiral metal-organic frameworks for asymmetric heterogeneous catalysis. Chem. Rev. **112**, 1196–1231 (2012)
10. Z. Yin, Q.X. Wang, M.H. Zeng, Iodine release and recovery, influence of polyiodide anions on electrical conductivity and nonlinear optical activity in an interdigitated and interpenetrated bipillared-bilayer metal-organic framework. J. Am. Chem. Soc. **134**, 4857–4863 (2012)
11. L. Hashemi, A. Morsali, Microwave assisted synthesis of a new lead(ii) porous three-dimensional coordination polymer: study of nanostructured size effect on high iodide adsorption affinity. CrystEngComm **14**, 779–781 (2012)
12. S. Qiu, G. Zhu, Molecular engineering for synthesizing novel structures of metal–organic frameworks with multifunctional properties. Coord. Chem. Rev. **253**, 2891–2911 (2009)
13. D. Zacher, O. Shekhah, C. Woll, R.A. Fischer, Thin films of metal-organic frameworks. Chem. Soc. Rev. **38**, 1418–1429 (2009)
14. M. Meilikhov, K. Yusenko, E. Schollmeyer, C. Mayer, H.-J. Buschmann, R.A. Fischer, Stepwise deposition of metal organic frameworks on flexible synthetic polymer surfaces. Dalton Trans. **40**, 4838–4841 (2011)
15. D. Zacher, K. Yusenko, A. Betard, S. Henke, M. Molon, T. Ladnorg, O. Shekhah, B. Schupbach, T. Arcos, M. Krasnopolski, M. Meilikhov, J. Winter, A. Terfort, C. Woll, R.A. Fischer, Liquid-phase epitaxy of multicomponent layer-based Porous coordination polymer thin films of [M(L)(P)0.5] type: importance of deposition sequence on the oriented growth. Chem. Eur. J. **17**, 1448–1455 (2011)
16. J.K. Yuan, X.G. Liu, O. Akbulut, J.Q. Hu, S.L. Suib, J. Kong, F. Stellacci, Superwetting nanowire membranes for selective absorption. Nanotechnology **3**, 332–336 (2008)
17. A.R. Abbasi, K. Akhbari, A. Morsali, Dense coating of surface mounted CuBTC metal–organic framework nanostructures on silk fibers, prepared by layer-by-layer method under ultrasound irradiation with antibacterial activity. Ultrason. Sonochem. **19**, 846–852 (2012)
18. V. Safarifard, A. Morsali, Application of ultrasound to the synthesis of nanoscale metal-organic coordination polymers. Coord. Chem. Rev. **292**, 1–14 (2015)
19. S. Hermes, F. Schröder, R. Chelmowski, C. Wöll, R.A. Fischer, Selective nucleation and growth of metal-organic open framework thin films on patterned COOH/CF3-terminated self-assembled monolayers on Au(111). J. Am. Chem. Soc. **127**, 13744–13745 (2005)
20. E. Biemmi, C. Scherb, T. Bein, Oriented growth of the metal organic framework $Cu_3(BTC)_2(H_2O)_3{\cdot}xH_2O$ tunable with functionalized self-assembled monolayers. J. Am. Chem. Soc. **129**, 8054–8055 (2007)
21. A. Schoedel, C. Scherb, T. Bein, Oriented nanoscale films of metal–organic frameworks by room-temperature gel-layer synthesis. Angew. Chem. Int. Ed. **49**, 7225–7228 (2010)
22. D. Zacher, A. Baunemann, S. Hermes, R.A. Fischer, Deposition of microcrystalline $[Cu_3(btc)_2]$ and $[Zn_2(bdc)_2(dabco)]$ at alumina and silica surfaces modified with patterned self assembled organic monolayers: evidence of surface selective and oriented growth. J. Mater. Chem. **17**, 2785–2792 (2007)
23. J. Gascon, S. Aguado, F. Kapteijn, Manufacture of dense coatings of $Cu_3(BTC)_2$ (HKUST-1) on α-alumina. Microporous Mesoporous Mater. **113**, 132–138 (2008)
24. A.M.B. Furtado, J. Liu, Y. Wang, M.D. LeVan, Mesoporous silica–metal organic composite: synthesis, characterization, and ammonia adsorption. J. Mater. Chem. **21**, 6698–6706 (2011)
25. Mercury 1.4.1, Copyright Cambridge Crystallographic Data Centre, 12 Union Road, Cambridge, CB21EZ, UK, 2001-2005
26. M.Y. Masoomi, K.C. Stylianou, A. Morsali, P. Retailleau, D. Maspoch, Selective CO_2 capture in metal-organic frameworks with azine-functionalized pores generated by mechanosynthesis. Cryst. Growth Des. **14**, 2092–2096 (2014)
27. A.R. Abbasi, A. Morsali, Formation of silver iodide nanoparticles on silk fiber by means of ultrasonic irradiation. Ultrason. Sonochem. **17**, 704–710 (2010)
28. M. Meilikhov, K. Yusenko, E. Schollmeyer, C. Mayer, H.-J. Buschmann, R.A. Fischer, Stepwise deposition of metal organic frameworks on flexible synthetic polymer surfaces. Dalton Trans. **40**, 4838–4841 (2011)
29. M.Y. Masoomi, S. Beheshti, A. Morsali, Shape control of Zn(II) metal–organic frameworks by modulation synthesis and their morphology-dependent catalytic performance. Cryst. Growth Des. **15**, 2533–2538 (2015)
30. R. Moosavi, A.R. Abbasi, M. Yousefi, A. Ramazani, A. Morsali, Ultrasound-assisted coating of polyester fiber with silver bromide nanoparticles. Ultrason. Sonochem. **19**, 1221–1226 (2012)
31. M.D. Luque de Castro, F. Priego-Capote, Ultrasound-assisted crystallization (sonocrystallization). Ultrason. Sonochem. **14**, 717–724 (2007)
32. A.R. Abbasi, A. Morsali, Synthesis and properties of silk yarn containing Ag nanoparticles under ultrasound irradiation. Ultrason. Sonochem. **18**, 282–287 (2011)
33. P. Horcajada, C. Serre, G. Maurin, N.A. Ramsahye, F. Balas, M. Vallet-Regi, M. Sebban, F. Taulelle, G. Ferey, Flexible porous metal-organic frameworks for a controlled drug delivery. J. Am. Chem. Soc. **130**, 6774–6780 (2008)
34. N.A. Khan, Z. Hasan, S.H. Jhung, Adsorptive removal of hazardous materials using metal-organic frameworks (MOFs): a review. J. Hazard. Mater. **244**, 444–456 (2013)